3D MIMO for 5G NR: Several Observations from 32 to Massive 256 Antennas Based on Channel Measurement

Jianhua Zhang, Zhe Zheng, Yuxiang Zhang, Jie Xi, Xiongwen Zhao, and Guan Gui

So far, 3D MIMO studies reported are mostly done with antenna elements from 32 up to 128 in the limited scenario at one frequency. To gain further insights into the 3D massive MIMO channel and performance, field measurements from 32 to 256 antenna elements at the transmitter and 16 antenna elements at the receiver are performed in three typical deployment scenarios, including outdoor to indoor, urban microcell, and urban macrocell at both 3.5 and 6 GHz frequencies with 200 MHz bandwidth.

Abstract

By placing active antennas in a 2D grid at a BS, 3D MIMO is considered as a promising and practical technique for 5G New Radio (NR). So far, 3D MIMO studies reported are mostly done with antenna elements from 32 up to 128 in the limited scenario at one frequency. To gain further insights into the 3D massive MIMO channel and performance, field measurements from 32 to 256 antenna elements at the transmitter and 16 antenna elements at the receiver are performed in three typical deployment scenarios, including outdoor to indoor, urban microcell, and urban macrocell at both 3.5 and 6 GHz frequencies with 200 MHz bandwidth. Based on the extracted channel information from measured data, power angle spectrum, root mean square angle spread, channel capacity, and eigenvalue spread have been studied. Several observations, including 3D MIMO channel spatial dispersive properties and multi-user performance varying with antenna number, scenario, and frequency are given. These findings can provide valuable experimental insights for efficient utilization of 3D MIMO with massive antenna elements.

Introduction

In recent years, researchers have focused their eyes on the fifth generation (5G) mobile communication system. As a new generation system we are looking forward to, 5G has many prospective advantages such as peak data rates of 10 Gb/s, user experienced data rate from 0.1 to 1 Gb/s, terminal latency reaching the millisecond level, and system capacity 1000 times that of the Long Term Evolution (LTE) system of today.

As one of the promising techniques for 5G New Radio (NR), massive multiple-input multiple-output (MIMO) will greatly increase the system capacity by deploying tens to hundreds of antennas at a base station (BS). In [1], it is theoretically proved that in massive MIMO with a simple channel conjugated pre-coder, intra-cell interference will vanish and high beamforming gain can be achieved. As the most feasible realization of massive MIMO, 3D MIMO extends the antenna array from only the azimuth plane to both azimuth and elevation planes, which helps to enhance the spatial resolution and improve the desired signal power and reduce the multi-user interference with the acceptable antenna size [2]. Reference [3] answer how much 3D MIMO meets our expectations in versatile 5G scenarios by conducting measurements with 56 × 32 antenna elements at 3.5 GHz with 100 MHz bandwidth. The results show that outdoor to indoor (O2I) is the most beneficial scenario, followed by urban microcell (UMi) and urban macrocell (UMa) scenarios.

System-level simulation of 3D MIMO with 32 antenna ports achieves 2–3.6 times gain in cell average throughput and 1.5–5 times gain in cell edge throughput compared to that of an LTE system with 2 antenna ports in [4]. A systematic design for a 3D MIMO product considering the restrictions of both baseband and hardware is proposed, and a field trial with 128 antenna elements at 2.6 GHz frequency with multi-user MIMO (MU-MIMO) validates that 3D MIMO meets the spectral efficiency requirement of the 5G enhanced mobile broadband services [5].

By deploying massive antenna elements, favorable propagation, which describes the pairwise orthogonality of the channel vectors from different users to the BS, has been assumed as an attractive advantage. However, in practical systems, users may be close to each other and share the common scatterers, so to what extent a "favorable propagation" condition can be realized in a real environment is of concern. Moreover, for the radio propagation properties varying with versatile scenarios and frequency bands, field channel measurements and studies play a vital role before the efficient deployment of 3D MIMO with massive elements for 5G NR. There are already some massive MIMO measurement campaigns considering MU-MIMO performance reported in the current literature. Researchers from Aalborg University conducted measurement at 5.8 GHz with 100 MHz and 64 antenna elements, and it was found that an increase in the antenna aperture would improve massive MIMO performance [6]. Lund University launched multi-user massive MIMO measurement at 2.6 GHz with a bandwidth of 50 MHz and 128 antenna elements in a residential area, and the results show that most of the predicted capacity gains of massive MIMO could be achieved at a reasonable number of antennas [7]. Reference [8] conducted a measurement with a uniform linear array (ULA) of 64 antenna elements in a center

Digital Object Identifier:
10.1109/MCOM.2018.1700846

Jianhua Zhang, Zhe Zheng, Yuxiang Zhang, and Jie Xi are with Beijing University of Posts and Telecommunications; Xiongwen Zhao is with North China Electric Power University; Guan Gui is with Nanjing University of Posts and Telecommunications.

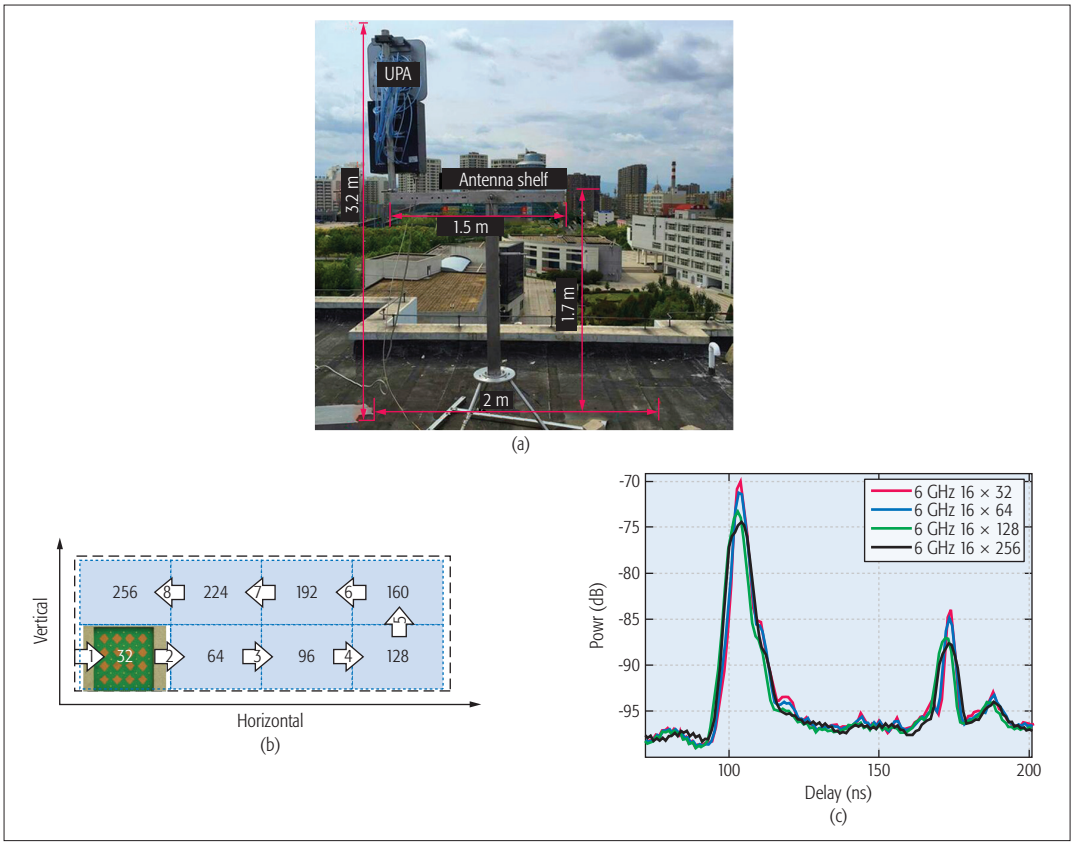

Figure 1. Shelf and principle of massive antenna array: a) Tx antenna shelf; b) principal diagram of 3D MIMO antennas from 32 to 256 at Tx; c) the PDPs of 32, 64, 128, and 256 Tx at 6 GHz.

hall for the stationarity investigation of massive MIMO, and a novel twin-cluster model including the spherical wavefront and a birth-death process was proposed for the massive MIMO channel [9].

It can be found that most of the reported measurements or trials are from 64 up to 128 antenna elements in the limited scenario at one frequency. To the best of the authors' knowledge, measurements of 3D massive MIMO with antennas above 128 are rare. The channel properties of 3D MIMO with massive antenna elements in real environments and their influence on 5G NR design are not well known. Thus, in this article, we attempt to investigate the channel characteristics and their performance in 3D MIMO with massive antenna elements in UMi, UMa, and O2I scenarios at both 3.5 and 6 GHz with 200 MHz bandwidth. A large-scale virtual antenna array in a 2D grid, with 256 elements at the transmitter (Tx) and two cylindric antenna arrays with 16 elements at each receiver (Rx), is utilized. The power delay profile (PDP) is drawn; then spatial alternating generalized expectation maximization (SAGE) is used to extract the channel parameters from the measured data. The spatial stochastic properties, including power angle spectrum (PAS) and root mean square (RMS) angle spread (AS), are investigated. Moreover, channel capacity and eigenvalue spread are studied. Finally, by performing a zero forcing block diagonalized (ZFBD) scheme, the MU-MIMO precoding capacity is also given to discuss the "favorable propagation" realization in a practical scenario under both line of sight (LoS) and non-LoS (NLoS) cases. The remainder of this article corresponds to the above.

Measurement Description

Measurement System

To investigate the propagation characteristics of a 3D MIMO channel with massive elements, the measured data are recorded by Elektrobit PropSound in such a way that a periodic pseudo random binary sequence (*m*-sequence) is transmitted over the air from Tx to Rx. PropSound works at a carrier frequency of either 3.5 or 6 GHz, with an effective bandwidth of 200 MHz. As is known, the frequency band around 3.5 or 6 GHz has been allocated to 5G trials in some regions and countries. The synchronization between the transmitting and receiving antennas is realized by a rubidium clock. A uniform antenna array (UPA) with 32 elements and an omnidirectional antenna array (ODA) with 56 elements at the carrier frequency of either 3.5 or 6 GHz are unitized in the measurement. The layout of the measurement antenna and detailed antenna parameters can be found in [3, Table 1 and Fig. 1].

In order to realize 256 antennas at the Tx, a UPA antenna array is installed and shifted at the antenna shelf, as shown in Fig. 1a. The UPA with 32 elements can shift vertically and horizontally in the shelf, which has two fixed groove sets with 0.5 wavelength of 3.5 and 6 GHz, so the alignment of the antenna array is guaranteed. Thus, antenna varying from 32, 64, 128, to 256 elements is virtually formed and is illustrated in Fig. 1b. A high-speed antenna switching unit is used at both the Tx and Rx sides to sound the Tx to Rx antenna pairs in one sampling cycle. Moreover, the campaigns are performed during

To investigate the propagation characteristics of 3D MIMO channel with massive elements, the measured data are recorded by Elektrobit PropSound by the way that periodic pseudo random binary sequence (m-sequence) is transmitted over the air from Tx to Rx. PropSound works at the carrier frequency of either 3.5 or 6 GHz, with an effective bandwidth of 200 MHz.

The classical parameter estimation scheme SAGE is used to extract the parameters of different propagation paths including propagation delay, Doppler shift, elevation angle of departure (EAoD), azimuth angle of departure (AAoD), elevation angle of arrival (EAoA) and azimuth angle of arrival (AAoA).

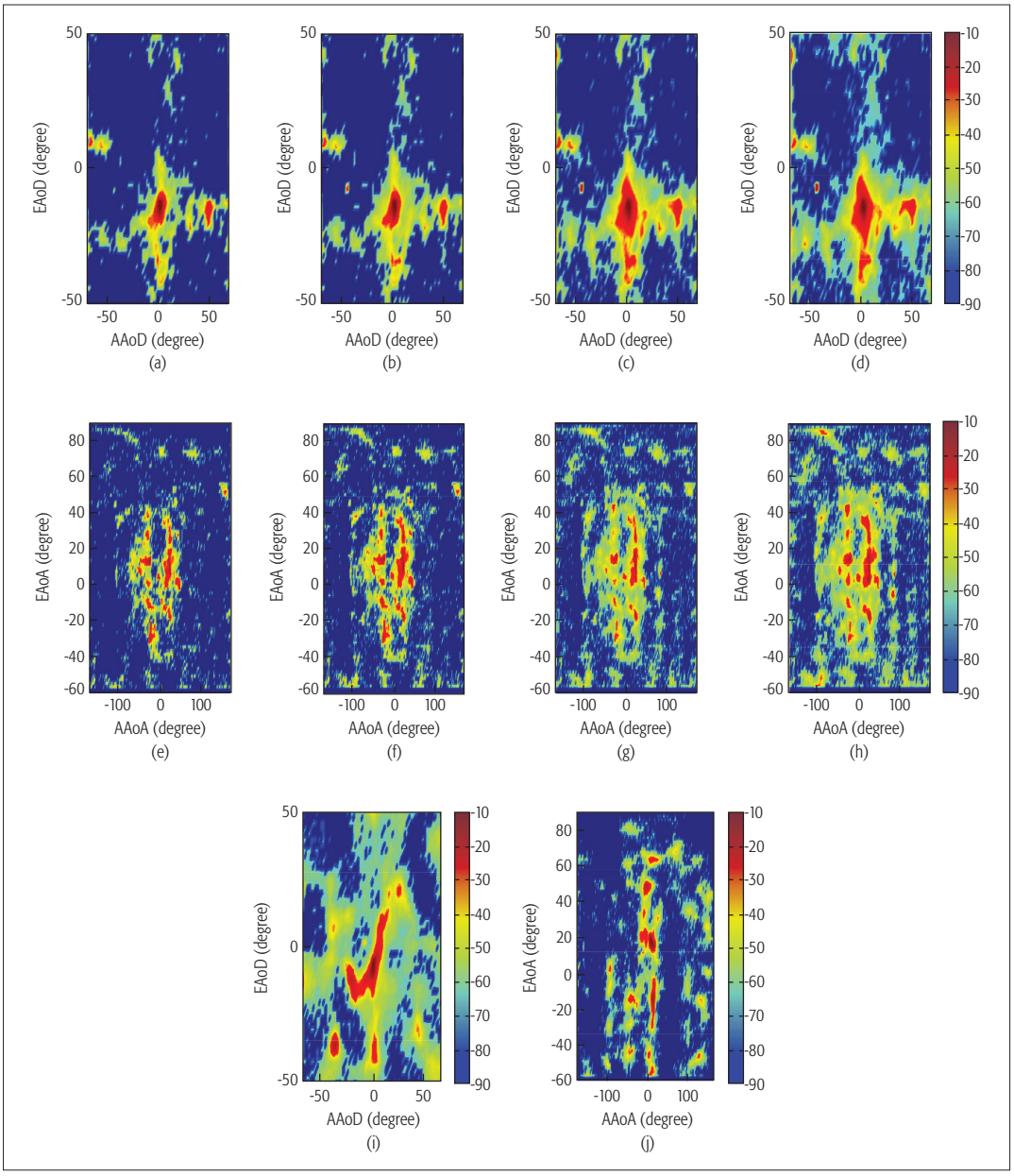

Figure 2. PAS in UMa LoS scenario: a) AoD of 6 GHz 32 Tx; b) AoD of 6 GHz 64 Tx; c) AoD of 6 GHz 128 Tx; d) AoD of 6 GHz 256 Tx; e) AoA of 6 GHz 32 Tx; f) AoA of 6 GHz 64 Tx; g) AoA of 6 GHz 128 Tx; h) AoA of 6 GHz 256 Tx; i) AoD of 3.5 GHz 256 Tx; j) AoA of 3.5 GHz 256 Tx.

summer vacation in order to make scatters static during the measurement. That is, few people and students are on campus at that time, which ensures that few occurring moving objects and human bodies when the channel measurement is conducted. Thus, a time quasi-stationary environment is guaranteed when the UPA array is shifted 8 times within one sampling cycle. The rationality of this virtual large-scale antenna measurement method from the point of spatial propagation properties is given in [10]. As for multi-user measurement, one ODA is equipped at Rx and 16 of 56 elements are active as one user. As for a second user, another ODA antenna is installed at 20 wavelengths away from the first user. The 6 GHz antennas have the same structure as the 3.5 GHz ones, and the antenna elements spacing is also half wavelength. To be noted, repeated measurements are conducted at 3.5 and 6 GHz by using the massive antenna arrays of the same structure as described above, which will allow us to compare the 3D MIMO with massive elements propagation characteristics among different measurement cases and also those of 56 × 32 antenna elements in [3].

Measurement Scenarios

Three typical measurement scenarios are chosen considering 3D MIMO with massive elements promising deployment scenarios and also interesting in standards. At each scenario, we repeat the measurement routes in both LoS and NLoS cases in order to get the statistical tendency and reliable observations. Due to space limitation, all measurement scenario maps and environments can be found in [3, Fig. 2]. In this article, the UMi scenario corresponds to UMi-BWC, the UMa is UMa-HF, and the O2I is O2I-KX in [3], respective-

ly. The Rx antenna array is placed on a trolley of 1.8 m height.

Channel Characteristics and Performance Analysis of 3D Massive MIMO

After field channel measurement, channel impulse response (CIR) can be obtained by correlating the received measured data with the transmitted known *m*-sequence. The classical parameter estimation scheme SAGE is used to extract the parameters of different propagation paths including propagation delay, Doppler shift, elevation angle of departure (EAoD), azimuth angle of departure (AAoD), elevation angle of arrival (EAoA), and azimuth angle of arrival (AAoA) [11]. In order to fully capture all dominant paths that exist in the measured scenario, 100 paths are estimated for each measurement cycle, namely, $L = 100$. We select the boresight of the antennas as the reference, that is, zero degree for both elevation and horizontal angles.

Power Delay Profile

It can be seen that cyclic prefix (CP) aided orthogonal frequency-division multiplex (OFDM) is adopted as the basis waveform and similar numerologies for 5G NR [12]. When antenna elements increase to 128 or more, will it affect those of 5G NR? The power delay profile (PDP) of CIR directly reflects the dispersions of multipath components (MPCs) in the delay domain; thus, the maximal delay and RMS delay spread can be calculated. Those values have the impact on the CP, subcarrier spacing of OFDM, and frame structure design of 5G NR. In order to understand how the increase of antenna number will influence the delay domain, we draw the PDPs by averaging the power of MPCs of 32, 64, 128, and 256 Tx antennas and 16 Rx antennas in Fig. 1c for one spot in UMa at 6 GHz as an example.

The measured CIR at time t can be written as $h(\tau_n, t)$, $n = 1, \cdots, N$, where τ_n indicates the delay of the nth sample in the delay domain. N is the sampling length of a CIR snapshot. Then the PDP corresponding to the CIR at time t can be calculated by

$$P(\tau_n, t) = ||h(\tau_n, t)||^2, \; n = 1, \cdots, N \qquad (1)$$

where $||\cdot||$ indicates 2-norm operation.

It can be observed from Fig. 1c that varying from 32 to 256 antenna elements, the peak value of PDP becomes nearly 5 dB lower (i.e., from −70 to −75 dB). Their shapes are slightly wider and flatter as antenna number increases. The reason is that the CIR of the same antenna pair from Tx to Rx has a similar envelope. However, as the antenna number is enhanced, there is a minor arriving delay shift; the averaging of CIR power with larger antenna number will lead to this phenomenon. In our measurement, the antenna is a 2D grid arrangement in order to avoid a too large azimuth plane; thus, the delay shift with antenna number is also minor. The power level of PDP −70 dB deep is caused by large-scale fading, and it will be normalized to 0 dB during capacity calculation in order to decouple the large-scale fading. The PDP consistency among 32, 64, 128, and 256 Tx antennas hints that the parameters related to the delay domain of 5G NR does not need to change greatly when enlarging the antenna number in both vertical and azimuth planes.

Power Angle Spread

Curiously, as the antenna number at the BS increases, how about the MPCs' power dispersion in the spatial domain, and at how high a degree can 3D MIMO take advantage of the massive antenna number? In order to answer this intuitively, power angle spectrum (PAS) is defined and investigated [3]. PAS will directly influence the spatial correlation of a channel and is helpful to observe the distribution of power in space.

In Fig. 2, the angle of arrival (AOA) and angle of departure (AOD) in both the horizontal and vertical planes of PAS with 32, 64, 128, and 256 BS antenna elements in the UMa LoS scenario are plotted. The abscissa indicates the azimuth angle, and the ordinate represents the elevation angle. The estimated power of each MPC is marked by color: red represents the strongest, yellow the middle, and blue the weakest. Seen from Figs. 2a–2h, in the 6 GHz case, for AOA, the power of AAoA distributes between −25° and 25°, and that of EAoA is between 0° and 40°. For AOD, the powers of AAoD and EAoD concentrate on 0° and −15°, respectively. The power of 32 Tx is mainly in the vicinity of these two areas. When increasing the antenna number, a clear tendency can be observed that the PAS will spread out. When it reaches 256 antenna elements at the BS, strong MPCs expand to most of the angle domains in Figs. 2d and 2h. This means that with increasing antenna element number, the antenna aperture will be enlarged. Then MPCs from wider vertical and horizontal planes can be received and estimated. Thus, the distribution of MPCs in 3D space is more dispersive. The tendency of MPC diffusion is 256 > 128 > 64 > 32. Thus, the spatial degree of freedom will be enhanced for such MPC dispersion. This finding is also the first experimental validation that the channel will tend to be low correlation when the antenna number increases in reality. Hence, increasing the antenna number at the BS is expected to improve the system capacity by fully utilizing the spatial domain, and quantitative results of capacity improvement are given later.

As some millimeter-wave channel research has been reported, the sparsity of MPCs in the delay and space domains is observed. So how about 3D MIMO channel below 6 GHz? For comparison, the AoA and AoD of PAS of 256 Tx in 3.5 GHz with the same Tx power in Figs. 2i and 2j. It can be found that the power of MPCs in 3.5 GHz is concentrated on nearly the same angle domain as 6 GHz. For the departure angle, AAoD of 3.5 GHz is very similar to that of 6 GHz, while EAoD of 3.5 GHz is much larger than that of 6 GHz. This can be explained by the fact that as frequency increases, the wavelength of radio waves becomes shorter, that is, from 8.57 to 5 cm with the frequency enhanced from 3.5 GHz to 6 GHz. However, in the elevation plane, the BS is much higher than the MS, and the larger objects such as high buildings are mainly scatterers. They make the power of MPCs of short wavelength paths decay severely, which is more beneficial

Curiously, as the antenna number at BS increases, how about the MPCs' power dispersion in spatial domain and how much degree that 3D MIMO can take advantage of massive antenna numbers? In order to answer this intuitively, power angle spectrum (PAS) will be defined and investigated. PAS will directly influence the spatial correlation of channel and is helpful to observe the distribution of power in space.

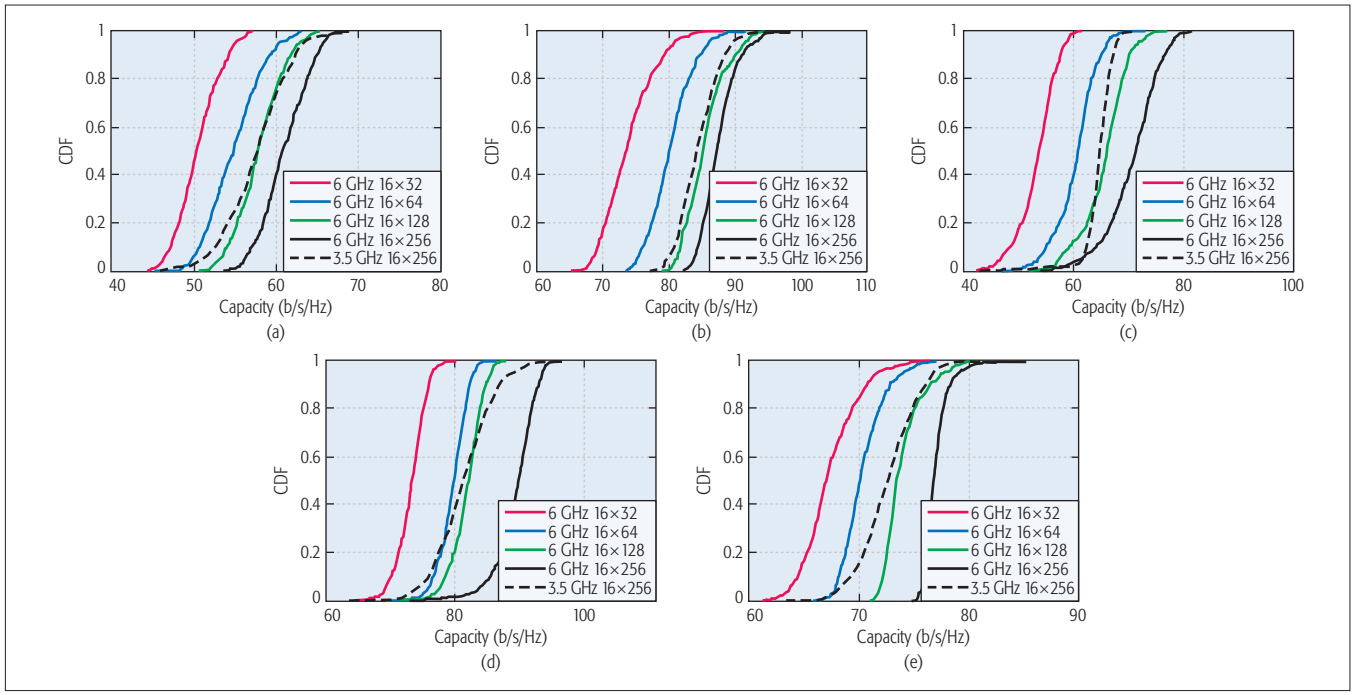

Figure 3. SU-MIMO capacity CDF of 32, 64, 128, and 256 Tx in different scenarios: a) UMi LoS; b) UMi NLoS; c) UMa LoS; d) UMa NLoS; e) O2I NLoS.

to the reflection and diffraction of radio waves at lower frequency. One interesting phenomenon is that the arrival angle of 3.5 GHz in Fig. 2j is more dense than that of 6 GHz in Fig. 2h. This is because more MPCs can be reflected and scattered by the small objects surrounding the MS for 6 GHz, the shorter wavelength, which leads to the PAS being more dispersive. In the next section, it is validated that the rich dispersion of arrival angle at 6 GHz will make the spatial correlation lower and bring higher capacity compared to that of 3.5 GHz. Considering the radio spectrum is valuable for mobile communication, frequency around 6 GHz is also very attractive for 5G NR due to the benefits of 3D massive MIMO with rich spatial dispersion.

RMS Angle Spread

In order to quantitatively know the angle dispersion in different scenarios and frequencies, angle spread (AS) is calculated. Four ASs are compared in this article, which are elevation angle spread of departure (ESD), elevation angle spread of arrival (ESA), azimuth angle spread of departure (ASD) and azimuth angle spread of arrival (ASA), respectively. Moreover, root mean square angle spread (RMS AS) is calculated as in 3GPP [13].

AS values in UMi, UMa, and O2I scenarios for both 3.5 and 6 GHz are summarized in Table 1. In comparison, the AS result of [3] with 32 Tx antenna elements and 3GPP TR 36.873 [13] are also listed. We consider the most promising scenario of 3D MIMO, O2I, first. Table 1 shows that all four ASs are very close, and only a minor increase can be observed from 32 to 256 antennas in the case of 3.5 GHz. The reason is that in the O2I scenario, the MS is indoor and surrounded by various and rich scatterers, like desks, chairs, computes, walls, and roof. It leads to a large AS value close to 32 antenna elements, and non-obvious AS variation can be expected by varying the antenna number. This observation hints that 3D MIMO performance is very stable in the O2I scenario, and even for an antenna with 32 elements, a high spatial degree of freedom can be achieved. Thus, it is still the most attractive deployment scenario for 3D MIMO. For UMi and UMa scenarios, ASD is very stable for 3.5 and 6 GHz with varying antenna numbers. However, ASA and ESA increase obviously in the case of 6 GHz and 256 Tx. For example, ESA in UMa is 1.08 (12°) and 1.15 (14°) for LoS and NLoS with 32 Tx at 3.5 GHz, while it increases to 1.36 (23°) and 1.42 (26°) with 256 Tx at 6 GHz, respectively. Thus, the angles of MPCs dramatically expand in the space domain as the Tx antenna number is enlarged. The reason is still the small scatterers around the MS. Then the shorter wavelength makes more MPCs be captured in the azimuth domain. Besides, we can observe that the value of ESD is larger in the case of higher frequency with shorter wavelength, which is the same as the results of PAS shown in Fig. 2.

SU-MIMO Channel Capacity

In this section, the wideband channel capacity [3] is calculated based on measured channel data in order to investigate the performance of 3D MIMO in reality.

Assuming signal-to-noise ratio (SNR) is 20 dB, the capacity CDFs of a 3D massive MIMO system (16 × 256) of 3.5 and 6 GHz are shown in Fig. 3. First, channel capacity is obviously improved by enhancing the antenna number. For example, for 5 percent capacity CDF in Fig. 3e, the capacity is 63, 68, 72, and 77 b/s/Hz at 32, 64, 128, and 256 antennas of the BS, respectively. This means that 22 percent relative improvement can be realized with the antenna element number varying from 32 to 256 antennas. Second, as shown in Figs. 3c and 3d, the capacity in the case of NLoS is higher than that in the case of LoS for the larger dispersion of

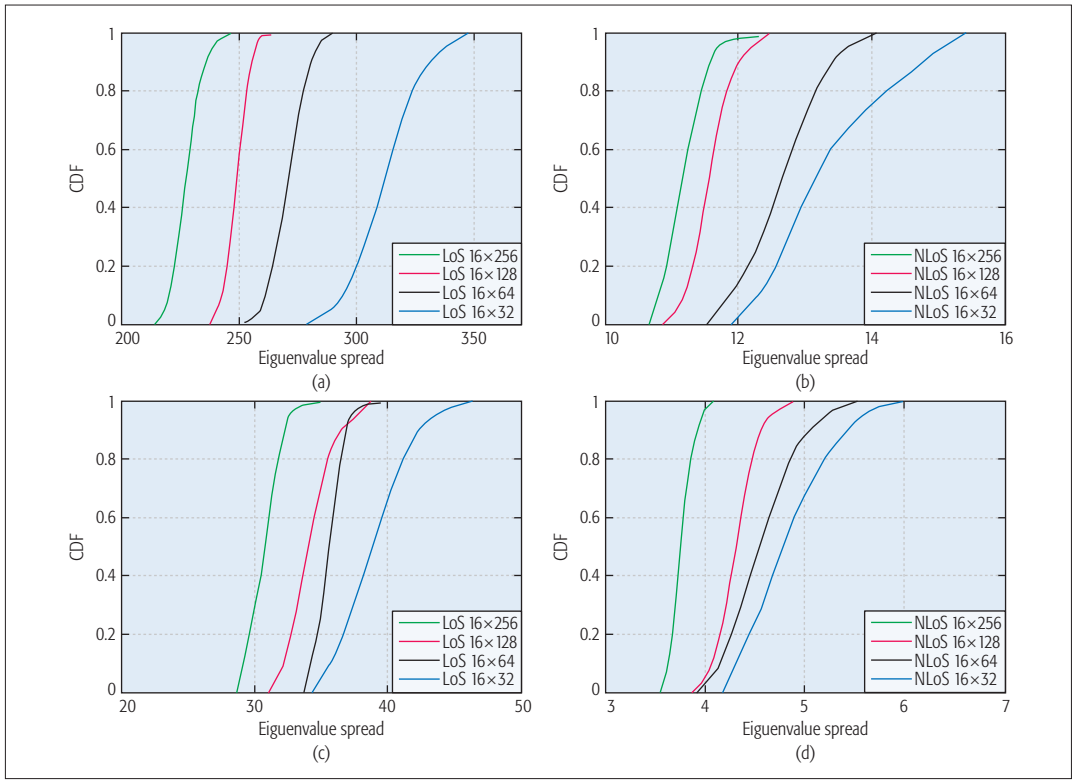

Figure 4. Eigenvalue spread in the UMa scenario: a) 3.5 GHz in LoS; b) 3.5 GHz in NLoS; c) 6 GHz in LoS; d) 6 GHz in NLoS.

The most attractive application scenario of 3D MIMO is multi-user case. By independent antenna elements being fed with different weighted multi-user signals, the high resolution mainlobe steering is achieved to distinguish users in the spatial domain. Thus the spatial orthogonality of users is expected to improve the multi-user capacity greatly for 5G NR.

MPCs in the angle domain in the case of NLoS. Moreoever, as plotted in Figs. 3a–3e, the capacity of 6 GHz is enhanced more obviously than that of 3.5 GHz. This is because the received power of 6 GHz is more spatially dispersive than that of 3.5 GHz, as shown in Figs. 2h and 2j, which makes the channel correlation of 6 GHz decrease rapidly.

Eigenvalue Spread

In order to study channel spatial correlation, the eigenvalues of antenna correlation are investigated. By applying fast Fourier transform (FFT) to the time-delay domain CIR matrix, the discrete time-frequency CIR is gotten as $\mathbf{H}(j, k)$ at time j and subcarrier k. Then its correlation matrix can be calculated by

$$\mathbf{R}(j, k) = \mathbf{H}(j, k)\,\mathbf{H}^{H}(j, k) \quad (2)$$

Here $(\cdot)^H$ is a Hermitian operation. Its eigenvalues can be obtained based on singular value decomposition to correlation matrix. In this article, the eigenvalue spread (ES) is defined to reflect the spatial dispersion. It can be expressed as

$$ES(j,k) = \frac{\max\left\{Eigen\left\{\mathbf{R}(j,k)\right\}\right\}}{\min\left\{Eigen\left\{\mathbf{R}(j,k)\right\}\right\}} \quad (3)$$

which is the ratio of the maximal and minimal eigenvalue. Larger value of $ES(j, k)$ means the channel power concentrates on the limited subchannels, and it cannot supply a high degree of freedom. A smaller value of $ES(j, k)$ means that the subchannels tend to be orthogonal, and it can provide more degrees of freedom to users.

As a typical 3D MIMO application scenario for a 5G system, we choose UMa to compare the results of ES with antenna number varying from 32, 64, 128, to 256 and frequency at 3.5 and 6 GHz. ES CDF of 3.5 GHz in the LoS case is given in Fig. 4a. It is clear that ES becomes smaller as antenna elements increase. The 5 percent ES CDF for 32, 64, 128, and 256 antenna elements at the BS are 280, 260, 240, and 220, respectively, and it decreases about 21.4 percent relatively from 32 to 256 antennas. Thus, increasing antenna number can make ES decrease remarkably, and the channel tends to be orthogonal. Then comparing among Figs. 4a–4d, we can see that ES of 6 GHz is smaller than that of 3.5 GHz, especially for the NLoS case (e.g., 10.5 and 3.5 for 5 percent ES CDF of 3.5 and 6 GHz). This result is consistent with the results of PAS in Fig. 2 and AS in Table 1. It is noted that ES in the case of NLoS is much smaller than that of LoS at both 3.5 and 6 GHz. The reason is NLoS has rich scatterers, which is consistent with the results of PAS and AS.

MU-MIMO Channel Capacity

The most attractive application scenario of 3D MIMO is the multi-user case. By independent antenna elements being fed with different weighted multi-user signals, high-resolution mainlobe steering is achieved to distinguish users in the spatial domain. Thus, the spatial orthogonality of users is expected to improve the multi-user capacity greatly for 5G NR. In this section, we compare the MU-MIMO ergodic capacity and classical ZFBD precoding capacity [14].

The result of ergodic capacity with variation of SNR is given in Fig. 5g. The way to calculate ergodic capacity of one user and two users can be found in [3, 15]. In the simulation, the two antenna elements that pick up the strongest signal

The MPCs becomes spatially dispersive as the Tx antenna number increases. However, such spatial dispersion will not ideally expand the capacity, thus the "favorable propagation" condition is not fully satisfied in the real channel measurement, considering the limitations from the user close position and shared scatters.

RMS AS (log10(°))			256 Tx				32 Tx [3]		3GPP [13]	
			3.5 GHz 200 MHz		6 GHz 200 MHz		3.5 GHz 100 MHz			
			LoS	NLoS	LoS	NLoS	LoS	NLoS	LoS	NLoS
UMi	ASA	μ	1.55	1.58	1.56	1.74	1.52	1.54	1.75	1.84
		σ	0.56	0.56	0.57	0.66	0.58	0.72	0.19	0.15
	ASD	μ	1.26	1.24	1.25	1.28	1.25	1.26	1.2	1.41
		σ	0.45	0.56	0.69	0.17	0.28	0.31	0.43	0.17
	ESA	μ	1.12	1.14	1.28	1.56	1.14	1.16	0.69	0.88
		σ	0.35	0.39	0.43	0.55	0.32	0.35	0.16	0.16
	ESD	μ	1.414	1.49	1.158	1.15	1.08	1.11	–	–
		σ	0.27	0.33	0.31	0.27	0.28	0.30	–	–
UMa	ASA	μ	1.52	1.64	1.66	1.92	1.46	1.59	1.81	1.87
		σ	0.38	0.76	0.57	0.65	0.39	0.65	0.20	0.11
	ASD	μ	1.21	1.31	1.31	1.32	1.27	1.02	1.15	1.41
		σ	0.35	0.34	0.23	0.31	0.32	0.32	0.28	0.28
	ESA	μ	1.23	1.18	1.36	1.42	1.08	1.15	0.95	0.26
		σ	0.54	0.68	0.66	0.50	0.19	0.25	0.16	0.16
	ESD	μ	1.48	1.46	1.31	1.22	1.08	1.03	–	–
		σ	0.23	0.14	0.18	0.15	0.22	0.18	–	–
O2I	ASA	μ	–	1.68	–	1.70	–	1.68	–	1.76
		σ	–	0.35	–	0.45	–	0.41	–	0.16
	ASD	μ	–	1.297	–	1.356	–	1.10	–	1.25
		σ	–	0.31	–	0.36	–	0.32	–	0.42
	ESA	μ	–	1.238	–	1.429	–	1.19	–	1.76
		σ	–	0.38	–	0.48	–	0.35	–	0.16
	ESD	μ	–	1.23	–	1.27	–	1.28	–	–
		σ	–	0.29	–	0.26	–	0.18	–	–

Table 1. RMS AS in different scenarios.

power in one ODA are selected as a practical user configuration, and the BS is constructed as shown in Fig. 1b, with all antenna elements in UPA. The capacity gap between one and two users is used as the performance improvement index, and defined as $(C_{2user} - C_{1user})/C_{1user}$. It can be observed that the capacity gap is relatively large for high SNR, which means that at high SNR we receive more MIMO multiplexing benefits. Thus, at high SNR range, multiplexing MIMO is still recommended to expand the 5G capacity greatly.

The capacity CDFs at medium-high SNR (20 dB) in the case of 3.5 and 6 GHz are given in Figs. 5a–5f. 54 and 48 percent improvement can be seen from 32 to 256 antennas at the BS with 2 users for the O2I scenario in 3.5 and 6 GHz, respectively. Thus, increasing antenna number from 32 to 64, 128, and 256, the channel capacity is improved remarkably in all cases. This result is consistent with ES, PAS, and AS. Moreover, it is worth noting that MU-MIMO certainly harvests much more than SU-MIMO does, for example, 35 and 54 percent increase from 32 to 256 antennas at the BS for the O2I scenario in 3.5 GHz with 1 and 2 users, respectively. It further validates that 3D massive MIMO is beneficial to the multi-user scenario with interference cancellation by precoding. Moreover, in all scenarios, the MU-MIMO capacity of 6 GHz is larger than that of 3.5 GHz, which is consistent with the results of SU-MIMO.

In order to investigate the favorable propagation, the MU-MIMO capacity varying with Tx and Rx antenna number is plotted in Figs. 5h and 5i. In comparison, the capacity of i.i.d. channel is also given. We know that if the "favorable propagation" condition holds, that is, if the propagation channels are spatially uncorrelated, the capacity of MU-MIMO will asymptotically approach to

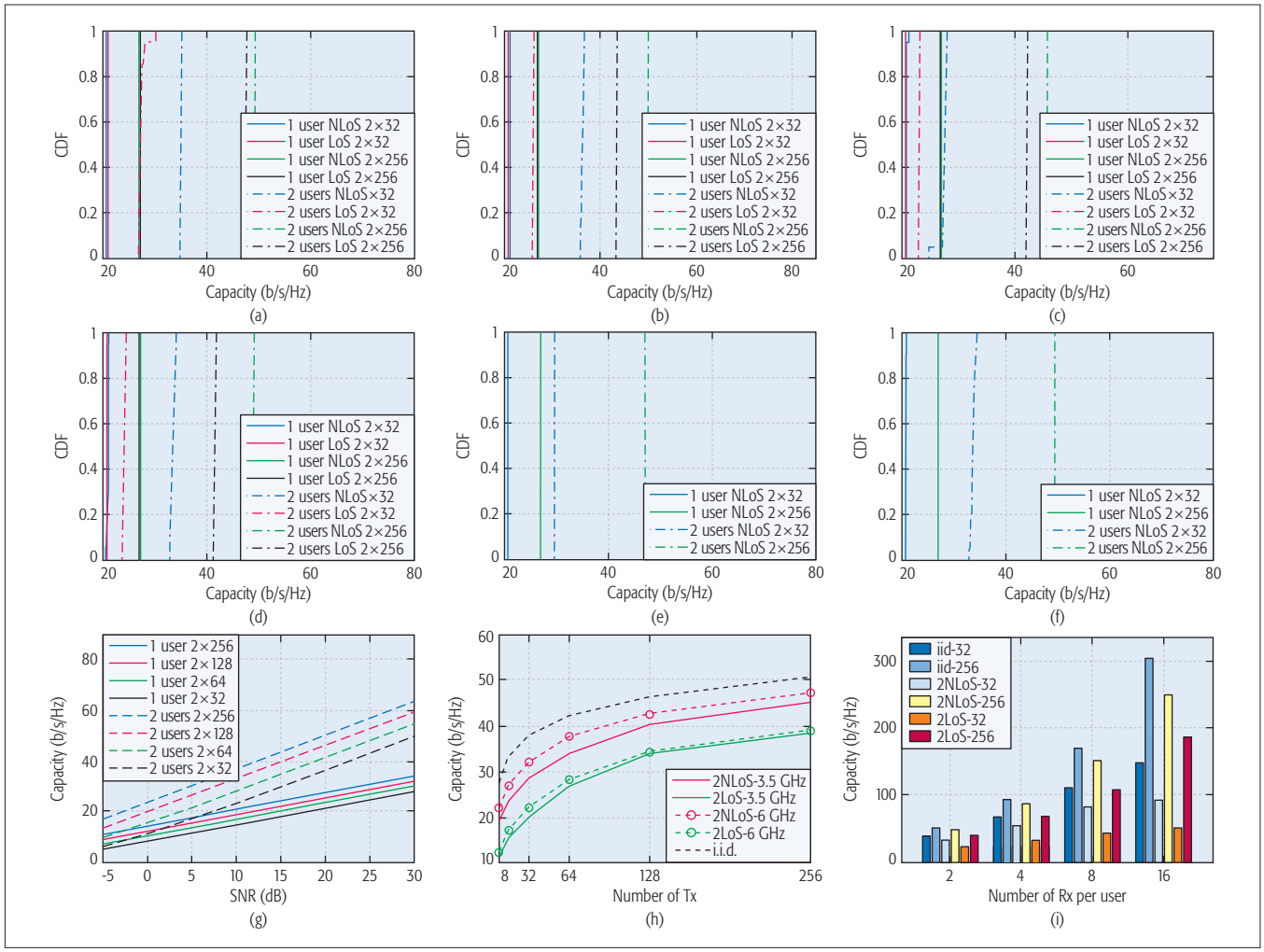

Figure 5. MU-MIMO capacity: a) capacity CDF of UMi at 3.5 GHz; b) capacity CDF of UMi at 6 GHz; c) capacity CDF of UMa at 3.5 GHz; d) capacity CDF of UMa at 6 GHz; e) capacity CDF of O2I at 3.5 GHz; f) capacity CDF of O2I at 6 GHz. ; g) Ergodic capacity of UMi at 6 GHz; h) capacity varying with Tx number; i) capacity varying with Rx number.

that of i.i.d.. From Fig. 5h, it is clearly found that the MU-MIMO capacity increases quickly with Tx antenna elements varying from 8 to 32, while it increases slowly after 64. It can be seen that the MU-MIMO precoding capacity reaches above 80 and 63 percent of i.i.d. for NLoS and LoS cases at 64 Tx, and above 85 and 73 percent of i.i.d. for NLoS and LoS cases at 128 Tx, respectively. And the capacity improvements for both cases by continuously increasing antenna number at Tx are less than 4.5 percent. Therefore, it is found that the improvements of MU-MIMO precoding capacity achieved by increasing BS antenna number slow down after it reaches 64 and gradually saturate at a certain value for all curves. There is still a minor gap between MU-MIMO precoding capacity and i.i.d. capacity even in the case of 256 antennas at Tx. As described earlier, the MPC becomes spatially dispersive as the Tx antenna number increases. However, such spatial dispersion will not ideally expand the capacity; thus, the favorable propagation condition is not fully satisfied in the real channel measurement, considering the limitations from the user close position and shared scatterers.

As shown in Fig. 5i, when the Tx number is fixed, increasing the Rx antenna number can also enhance the precoding capacity obviously. When varying Rx antenna number from 2 to 4, 8, and 16 with the Tx antenna number of 32, the precoding capacity of MU-MIMO can be improved from 22.3 to 31.8, 42.4, and 50 b/s/Hz, respectively. Obviously, the better performance will be obtained when both Tx and Rx numbers are enlarged; for example, the precoding capacity of 256 Tx with 16 Rx is 8.34 times than that of 32 Tx with 2 Rx. However, a certain capacity gap from the i.i.d. channel still exists for the imperfections in real measurements.

Conclusion

In order to investigate 3D massive MIMO experimentally, we conduct 2D grid antenna channel measurements in UMi, UMa, and O2I scenarios at both 3.5 and 6 GHz with 200 MHz bandwidth and antenna elements varying from 32 to 256. Comparative results including PAS, AS, SU-MIMO and MU-MIMO channel capacity, and eigenvalue spread have been investigated. The observations based on 3D massive MIMO channel measurement can be summarized as:

Antenna Number: As the antenna number increases, minor PDP difference is observed. Thus, the parameters related to the delay domain of 5G NR do not need to be changed greatly for 3D massive MIMO. But PAS of 3D massive MIMO

Increasing the number of antennas from 32 to 64, 128, and 256, the channel capacity is improved remarkably at both 3.5 and 6 GHz frequencies, for example, 54 and 48 percent increase from 32 to 256 antennas at a BS with two users for the O2I scenario at 3.5 and 6 GHz, respectively.

becomes more dispersive, and AS becomes larger in the angle domain. Especially in the azimuth plane, MPCs are widely distributed, which leads to a remarkable improvement of channel capacity.

Frequency: As the carrier frequency increases, the wavelength becomes shorter. More reflections will be caused by small objects and scatterers around an MS, which leads to a higher angular spread at the MS. However, the elevation angle is more dispersive at low frequency due to the high and large objects in the elevation plane of the BS, which have a stronger ability to reflect the long radio waves. This leads to the capacity and eigenvalue of 6 GHz being better than that of 3.5 GHz; that is, the performance of 3.5 GHz with 256 antennas at the BS is similar to that of 6 GHz with half of 256 antennas, 128 antennas. Considering the scarcity of frequency, frequencies higher than 3.5 GHz are also very attractive for 5G NR.

Scenarios: For the O2I scenario, channel capacity is relatively stable with the variation of frequency and antenna number. For the UMi and UMa scenarios, it can be observed that a remarkable increase is achieved at the higher frequency and larger antenna number. Especially for the UMa scenario, the larger antenna aperture is helpful to capture more MPCs, which leads to an increase in channel capacity. Those scenarios can take advantage of 3D massive MIMO in order to meet 5G's high spectral efficiency requirement.

MU-MIMO Performance: Increasing the number of antennas from 32 to 64, 128, and 256, the channel capacity is improved remarkably at both 3.5 and 6 GHz frequencies, for example, 54 and 48 percent increase from 32 to 256 antennas at a BS with two users for the O2I scenario at 3.5 and 6 GHz, respectively. This provides a hint that for the MU-MIMO scenario, even with the simple ZFBD algorithm used in this article, capacity can be increased dramatically by increasing the number of antennas at the BS. However, as the BS antenna number grows larger than 64, the MU-MIMO performance improvement is not as obvious as the favorable propagation is not ideally satisfied. Finally, increasing the Rx antenna number per user is also a feasible way to improve the precoding capacity. As an antenna technique development, 3D massive MIMO is certainly promising to be deployed to further improve 5G NR multi-user performance.

Acknowledgment

This research is supported in part by theNational Natural Science Foundation of China (No. 61781260394, 61322110), in part by the Key Program of Beijing Municipal Natural Science Foundation (No. L172030), in part by the National Science and Technology Major Program of the Ministry of Science and Technology (2018ZX03001031, 2017ZX03001028003), in part by the Ministry of Education — China Mobile Research Fund (No. MCM20160105), and in part by the Knowledge Innovation Program of Shenzhen (Ji20170134). This research is also supported by Huawei Technologies Co., Ltd..

References

[1] T. L. Marzetta, "Noncooperative Cellular Wireless with Unlimited Numbers of Base Station Antennas," *IEEE Trans. Wireless Commun.*, vol. 9, no. 11, Nov. 2010, pp. 3590–3600.
[2] J. H. Zhang, *et al.*, "Three-Dimensional Fading Channel Models: A Survey of Elevation Angle Research," *IEEE Commun. Mag.*, vol. 52, no. 6, June 2014, pp. 218–26.
[3] J. H. Zhang, *et al.*, "3D MIMO: How Much Does It Meet Our Expectations Observed from Massive Channel Measurements?" *IEEE JSAC*, vol. 35, Aug. 2017, pp. 1887–1903.
[4] Y.-H. Nam, *et al.*, "Full-Dimension MIMO (FD-MIMO) for Next Generation Cellular Technology," *IEEE Commun. Mag.*, vol. 51, no. 6, June 2013, pp. 172–79.
[5] G. Y. Liu, *et al.*, "3-D-MIMO with Massive Antennas Paves the Way to 5G Enhanced Mobile Broadband: From System Design to Field Trials," *IEEE JSAC*, vol. 35, no. 6, June 2017, pp. 1222–33.
[6] A. O. Martínez, E. De Carvalho, and J. Ø. Nielsen, "Towards Very Large Aperture Massive MIMO: A Measurement Based Study," *Proc. IEEE GLOBECOM Wksp.*, 2014.
[7] X. Gao *et al.*, "Measured Propagation Characteristics for Very-Large MIMO at 2.6 GHz," *Proc. 46th Annual Asilomar Conf. Signals Sys. Comp.*, 2012.
[8] L. Liu *et al.*, "Stationarity Investigation of a Los Massive MIMO Channel in Stadium Scenarios," *Proc. IEEE VTC-Fall*, 2015.
[9] S. Wu, *et al.*, "A Non-Stationary 3-D Wideband Twin-Cluster Model for 5G Massive MIMO Channels," *IEEE JSAC*, vol. 32, no. 6, June 2014, pp. 1207–18.
[10] H. Yu *et al.*, "The Rationality Analysis of Massive MIMO Virtual Measurement at 3.5 GHz," *Proc. IEEE ICCC Wksp.*, 2016.
[11] B. H. Fleury, *et al.*, "Channel Parameter Estimation in Mobile Radio Environments Using the SAGE Algorithm," *IEEE JSAC*, vol. 17, no. 3, Mar. 1999, pp. 434–50.
[12] S. Y. Lien *et al.*, "5G New Radio: Waveform, Frame Structure, Multiple Access, and Initial Access," *IEEE Commun. Mag.*, vol. 55, no. 6, June 2017, pp. 64–71.
[13] 3GPP Tech. Rep. 36.873, "Study on 3D Channel Model for LTE (Release 12)," Sept. 2014.
[14] Q. H. Spencer, A. L. Swindlehurst, and M. Haardt, "Zero-Forcing Methods for Downlink Spatial Multiplexing in Multiuser MIMO Channels," *IEEE Trans. Signal Processing*, vol. 52, no. 2, Feb. 2004, pp. 461–71.
[15] J. J. Gao *et al.*, "Performance Evaluation of Closed-Loop Spatial Multiplexing Codebook Based on Indoor MIMO Channel Measurement," *Int'l. J. Ant. Propagation*, vol. 2012, no. 701985, Oct. 2012, pp. 246–57.

Biographies

Jianhua Zhang [SM'12] is the Drafting Group (DG) Chairwoman of the ITU-R IMT-2020 channel model. She received her Ph.D. degree in circuits and systems from Beijing University of Posts and Telecommunication (BUPT) in 2003 and is now a professor at BUPT. Her current research interests include 5G, artificial intelligence, data mining, especially in massive MIMO and millimeter wave channel modeling, channel emulator, OTA test, and so on.

Zhe Zheng received his B.S. degree from Xiamen University and his M.S. degree from Guilin University of Electronic Technology. He is currently pursuing a Ph.D. degree in information and communication engineering at BUPT. His current research interests include channel modeling, 3-D MIMO, and massive MIMO.

Yuxiang Zhang received his B.S. degree in electronic information engineering from Dalian University of Technology in 2014. He is currently pursuing a Ph.D. degree in information and communication engineering at BUPT. His current research interests include channel modeling, 3-D MIMO, and machine learning.

Jie Xi received her B.S. degree in electronic information engineering from Jinan University in 2013. She is currently pursuing an M.S. degree at the School of Information and Communication Engineering, BUPT. Her research interests include channel modeling, 3-D MIMO, and massive MIMO.

Xiongwen Zhao [SM'06] received his Ph.D. degree in 2002 with high honors from Helsinki University of Technology (TKK), Finland. He is now a professor in wireless communications at North China Electric Power University in Beijing and chairs several projects by the National Science foundation of China (NSFC), State Key Laboratories, and companies on channel measurements, modeling, and simulations.

Guan Gui [SM'17] received his Dr.Eng. degree in information and communication engineering from University of Electronic Science and Technology of China, Chengdu, in 2011. He is now a professor with Nanjing University of Posts and Telecommunications, China. He has been/is an Editor for *Security and Communication Networks* (2012–2016), *IEEE Transactions of Vehicular Technology* (2017–), and *KSII Transactions on Internet and Information Systems*.